JOURNAL OF GEOPHYSICAL RESEARCH: ATMOSPHERES, VOL. 118, 3506–3519, doi:10.1002/jgrd.50249, 2013

Baffin Island snow extent sensitivity: Insights from a regional climate model

Mira Berdahl and Alan Robock

Received 4 September 2012; revised 17 December 2012; accepted 22 January 2013; published 8 May 2013.

[1] Recent modeling efforts suggest that the Little Ice Age (LIA) onset could be explained by a series of four large decadally-spaced volcanic eruptions. At that time, glaciers on Baffin Island advanced and did not retreat until the past century, perhaps due to Arctic and North Atlantic Ocean sea ice feedbacks. To try to determine what parameters sustain snow cover, we investigate the relative impacts of changes in radiation and advection on minimum summer snow extent over Baffin Island. We used the Weather Research and Forecasting (WRF) model to run eight 6 month long (April-September), 10 km resolution simulations, in which we varied boundary condition temperatures, solar radiation, and sea ice cover. Although the Control Run underestimated cloud cover and thus produced an exaggerated diurnal 2 m temperature cycle, the relative changes of snow extent show that WRF accurately simulates snow expansion into the same regions as during the LIA. With an average temperature decrease from current temperatures by -3.9 ± 1.1 K, it only requires one season for the model to lower the snowline by comparable elevation changes seen during the descent into the LIA. WRF's maximum snow line sensitivity is 7 K/km, within the range of the typically assumed lapse rate of 5–7 K/km in the Canadian Arctic. Thus, if a shift in the Arctic climate greatly expanded sea ice coverage following large volcanic eruptions, this would have been enough to perpetuate an ice sheet on Baffin Island throughout the LIA.

Citation: Berdahl, M., and A. Robock (2013), Baffin Island snow extent sensitivity: Insights from a regional climate model, *J. Geophys. Res. Atmos.*, *118*, 3506–3519, doi:10.1002/jgrd.50249.

1. Introduction

[2] The Little Ice Age (LIA) occurred in fits and starts between the 13th and 19th centuries, although clues from the field suggest regional variability in both timing and degree. In the Arctic, the LIA caused expansion of ice caps and glaciers to their largest extents in the past 8000 years [*Miller et al.*, 2010], but it is still unclear what triggered and sustained the transition into a colder climate. Field studies since the 1960s have noted that in areas of Baffin Island, in the eastern Canadian Arctic, sparse lichen cover over large areas could indicate that widespread glacierization was so recent that little recolonization had yet taken place [*Ives*, 1962; *Andrews et al.*, 1972; *Williams*, 1978a]. In north central Baffin Island, the terrain is a shallowly undulating plateau with an elevation range of 400–700 m [*Andrews et al.*, 1972]. Lowering the snow line into this zone could cause a drastic increase in area of snow coverage, and this region of Baffin Island is where the LIA snow expanded and could even have been where the Laurentide ice sheet originated [*Miller*, 1973; *Williams*, 1978a]. It is thus important to understand the sensitivity of snow cover to temperature changes in a highly responsive region such as Baffin Island.

[3] Proxy-based evidence recently collected from northern Baffin Island suggests that a sudden expansion of ice caps began soon after a succession of several large eruptions in the 13th century, the approximate onset of the LIA [*Anderson et al.*, 2008; *Geirsdóttir et al.*, 2009; *Zhong et al.*, 2010; *Miller et al.*, 2012]. The ice sheets did not start to melt until roughly a century ago. Using the Community Climate System Model-3 at T42 (about 2.8°) horizontal resolution, *Zhong et al.* [2010] found that it was possible to induce long-term North Atlantic wide cooling with only transient volcanic aerosol forcing. The mechanism found in the model to account for this widespread drop in temperature was a coupled sea ice-ocean feedback, wherein an expanded sea ice state perpetuated the typically short-lived effects of explosive volcanism [*Robock*, 2000]. An expanded sea ice state following volcanic eruptions is further supported by observations in Hudson Bay and Hudson Strait (the waters along the southern coast of Baffin Island). Ship records suggested that severe summer ice occurred in the years immediately following large volcanic eruptions during the 19th century [*Catchpole et al.*, 1989]. Entombed vegetation collected from the margins of ice caps in north central Baffin Island and analyzed by *Miller et al.* [2012] suggests two periods during the descent into the LIA with sudden advances in snow line. The first, from 1275

[1]Department of Environmental Sciences, Rutgers University, New Brunswick, New Jersey, USA.

Corresponding author: M. Berdahl, Department of Environmental Sciences, Rutgers University, 14 College Farm Road, New Brunswick, NJ 08901, USA. (mberdahl@envsci.rutgers.edu)

©2013. American Geophysical Union. All Rights Reserved.
2169-897X/13/10.1002/jgrd.50249

to 1300 CE, reveals sites in an elevation range of 660–1000 m and the second from 1430 to 1455 CE from sites in a range of 660–900 m elevation. That is, there was a sudden drop in snow line by about 300 m in a matter of only a few decades. Since the most reliable summer temperature proxies at high northern latitudes are glaciers, where 90% of their mass balance variation can be explained by summer temperature [*Koerner*, 2005], ice cap advances or recessions inform us about the local summer temperature. Based on these proxy climate reconstructions and their previous climate modeling results, *Miller et al*. [2012] suggested that the LIA onset was an abrupt event late in the 13th century which intensified later in the 15th century and that it could be explained by repeated explosive volcanism.

[4] These observations motivated us to investigate how sensitive the snow line elevation is; specifically, what are the relative impacts of changes in radiation or advection on minimum summer snow extent over Baffin Island? We used a high-resolution regional climate model to allow improved representation of atmospheric and snow processes given the steep and complex terrain of Baffin Island. We present results from eight unique 6 month long high-resolution simulations with imposed atmospheric temperature, solar constant, and sea ice perturbations, which are aimed to simulate what conditions may have led to the lowering of the snow line on Baffin Island. The experiments are designed to simulate a conditions likely to have occurred after a series of volcanic eruptions, such as a reduction in cooling and surface radiation, and the expansion of sea ice. We ran all the simulations from April through September to capture the full spring thaw through to the early fall.

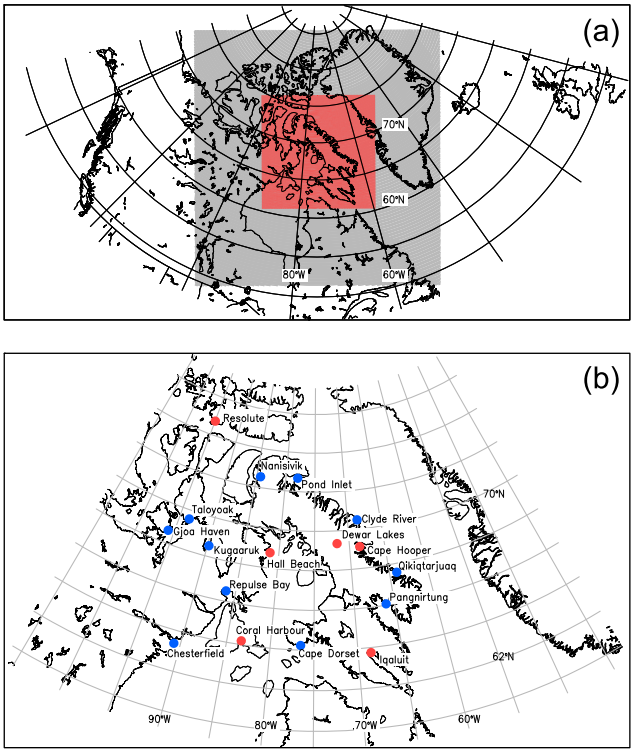

Figure 1. (a) Map of WRF domains, where parent domain (grey) has 30 km resolution and child domain (red) has 10 km resolution. (b) Automatic weather station locations, where red circles denote hourly data available and blue denote only daily average records available.

2. Model, Experiments, and Data

2.1. Model Description

[5] We used the Advanced Research Weather Research and Forecasting (WRF-ARW) regional weather and climate model version 3.3 [*Skamarock et al*., 2008] for all simulations. The ARW core was chosen as it is used as a research tool at the National Center for Atmospheric Research, as opposed to the non-hydrostatic mesoscale model core that is used operationally at the National Centers for Environmental Prediction. The 2-way nested model was fixed for all experiments, with a parent domain of 30 km horizontal resolution encompassing much of northern Canada and Greenland, and the inner domain of 10 km resolution, hedging Baffin Island (Figure 1a). There were 27 vertical levels in the WRF runs, with a model top at 50 mb.

[6] Each WRF simulation was run during the 6 month period of April-September 2005, a year without a strong North Atlantic Oscillation signal, typical Arctic minimum sea ice extent given the current decline, and relatively abundant remotely sensed data available. The results were compared to snow, cloud, and surface meteorological observations. Following *Hines et al*. [2011], we forced all runs with initial and boundary conditions from the National Centers for Environmental Prediction Global Forecasting System Final Analysis (GFS-FNL), which has a resolution of $1^\circ \times 1^\circ$. GFS-FNL provides input to WRF every 6 h of model time, and the time step in WRF is 120 s.

[7] The following parameterizations were used for all runs:

[8] 1. Noah land surface model (LSM) [*Chen and Dudhia*, 2001]

[9] 2. WRF Single Moment 5-class microphysics scheme [*Hong et al*., 2004]

[10] 3. Yonsei University planetary boundary layer scheme [*Hong et al*., 2006]

[11] 4. Goddard shortwave scheme [*Chou and Suarez*, 1994]

[12] 5. Rapid Radiative Transfer Model longwave scheme [*Mlawer et al*., 1997]

[13] 6. Kain Fritsch (new Eta) cumulus scheme [*Kain*, 2010]

[14] These parameterizations were chosen after we ran a set of 1 month long sensitivity tests for July of 1981, where we tested variations of parameterization choices and found that this combination did a good job of reproducing the climate for one summer month in the region. A very similar combination of parameterization choices is recommended by *Hines and Bromwich* [2008] based on the performance of their Polar WRF experiments over the Greenland Ice Sheet. All of our simulations applied spectral nudging to the u and v windfields above the boundary layer (about 1500 m altitude) to only the parent domain (the larger, 30 km resolution domain (Figure 1a)) as recommended by *Miguez-Macho et al*. [2004], since it has been shown to improve performance of Polar WRF [*Cassano et al*., 2011]. By nudging the u and v components of the wind, we maintain realism in the simulation while allowing temperature to remain a free parameter, since we want it to be predicted by the model.

[15] Sea ice in the model is prescribed by the GFS boundary conditions, updated every 6 h of model time. Sea ice in WRF V3.3 is handled by the Noah LSM, and is treated much the same as land. The sea ice has a fixed thickness of 3 m, and is divided into four layers just as the land surface is, with thermal conductivities modified from land-relevant values to ice-relevant values. Sea ice in the model is always 100% snow covered, and the skin temperature above the ice is then calculated above the snow in the same way it is calculated over snow-covered land. Versions Polar WRF 3.2 and standard WRF 3.2.1 could not complete the full 6 month simulation without crashing with unexplained segmentation faults. When the domain boundaries were placed in regions without strong topography, standard WRF 3.3 ran without problems, so this was the version used for all of our simulations.

2.2. Experimental Approach

[16] Since we are interested in sensitivity of snow extent to temperature perturbations, we performed eight experiments, the first of which was a Control Run where the model was forced with the GFS input data for the given time period. Four temperature experiments were run where the boundary conditions of the Control Run were perturbed for the full simulation by −1.5 K, −3 K, −4.5 K, and −6 K, and labeled the WRF −1.5 K, WRF −3 K, WRF −4.5 K, and WRF −6 K runs. By perturbing only the temperature of air in these runs, we only change one variable at a time, and thus, we know that any effects seen are purely from the advection of cooled air. However, we acknowledge that cooler air advected into the domain should be drier as well, but we did not remove moisture when cooling the boundaries. The model takes care of this "extra" moisture on its own by raining out at the boundaries of the parent (outer) domain so that air advected to the inner domain is drier in the cooled experiments than the Control Run. This drying effect increases with increasing temperature perturbation, as it should.

[17] In the sixth experiment, we ran the Control Run again, but with the solar constant set to 1301 W/m^2, 95% of its current value, labeled 95SOLCON. This is approximately a −12 W/m^2 change in radiative forcing at the tropopause, about three times the effect immediately following the 1991 Mount Pinatubo eruption [*McCormick et al*., 1995]. This run is another approach to cooling the domain, where instead of applying temperature perturbations to the boundary conditions only, in which the magnitude dissipates as it propagates into the inner domain, a uniform perturbation is applied across the entire domain. It must be noted, however, that this experiment represents only a lower bound on the effects of such a reduction in solar radiation since the boundary conditions feeding WRF are not subjected to the same reduction in radiation.

[18] Motivated by the results from *Zhong et al*. [2010], where an expanded sea ice state was induced and sustained after four sequential volcanic eruptions took place in the 13th century, we ran the simulation with sea ice fixed to the 1 April state for the full 6 months (labeled FixedSI). Finally, we ran a simulation where we both applied the −3K temperature perturbation to the boundaries and fixed the sea ice to the 1 April state (WRF −3K and FixedSI). We hypothesized that this final run would allow the cooled boundary temperatures to remain colder as winds were advected across the sea ice and would represent more realistic LIA-type conditions where temperature drops and expanded sea ice occur in concert.

2.3. Data

[19] In situ Environment Canada Automatic Weather Stations (AWS) observations in Nunavut, in addition to being sparse, tend to be biased toward low elevations, as most stations are along the coastline. This limits our ability to evaluate our high-resolution model output, but at the same time illustrates the necessity for running such models as a way to fill the gap in surface observations across the Island's interior. Here we focused on near-surface summer temperature output from the model, as it has been found to be the primary driver of high latitude glacier mass balance throughout most of the Holocene in parts of the eastern Canadian Arctic [*Koerner*, 2005].

[20] In addition to temperature, we evaluated the evolution of snow cover extent. We compared our model runs to the 4 km resolution Interactive Multisensor Snow and Ice Mapping System (IMS) satellite snow and sea ice cover daily data, from the National Climatic Data Center [*National Ice Center*, 2008], and Moderate Resolute Imaging Spectroradiometer (MODIS) Cloud Gap-Filled (CGF) Daily Snow Product at 0.5° horizontal resolution. As *Brown et al*. [2010] described, the IMS product is generated by trained analysts who use snow cover information from satellites, station observations, and passive microwave readings to create 4 km resolution maps for the entire Northern Hemisphere. Any cell containing more than 50% snow cover is classified as snow-covered. Since the product is predominantly derived from visible satellite imagery, it can be misleading during days of high cloud cover, a common occurrence during Arctic spring and summer. IMS maps have been documented to produce excessive snow cover fractions over the Arctic during the spring melt period. This artifact has been attributed to high cloud cover and less frequent satellite coverage over the Arctic [*Wang et al*., 2005a; *Brown et al*., 2007]. *Wang et al*. [2005a] also commented that the analysts have been trained to be "very aggressive" with their snow cover classification, often designating areas of patchy snow as completely snow-covered.

[21] We also used the MODIS CGF snow product for comparison to WRF, which is available between October and mid-June, and provides a daily snow coverage map irrespective of cloud cover [*Hall et al*., 2010]. The product provides a snow-cover map based on the most recent clear-sky observation and gives each cell a confidence based on the number of days since the last recorded view.

[22] Comparison of 10 km average (WRF), 4 km average (IMS), and point measurements (weather stations) should be interpreted with care. Area-averaged snow cover and temperature can be skewed in steep terrain. Much of Baffin Island's coastline is dramatic and contains sudden transition from sea level to high mountains and deeply carved fjords. Since most station locations are along the coast, low resolution grid cells would tend to smooth the transition from ocean to steep land. In their WRF modeling study of the Colorado Rockies, *Ikeda et al*. [2010] found that snowfall decreased at high elevations as model resolution became coarser. Since the higher resolution (2 km and 6 km) runs

resolved the higher peaks in the mountain range, cooler conditions are simulated and thus snow lasted longer on the peaks than the lower resolution (18 km and 36 km) runs. We chose 10 km resolution in an effort to approach the high resolution suggested by *Ikeda et al*. [2010] while conserving computation expenses.

[23] *Gardner et al*. [2009] derived an average ablation season lapse rate of 4.9 K/km from four ice caps in the Canadian Arctic. However, near-surface lapse rates over melting glaciers are often lower than those over land [*Greuell and Böhm*, 1998]. Thus, when comparing WRF to station data, we corrected surface temperatures produced by WRF with a standard lapse rate of 6 K/km [*Lucas-Picher et al*., 2012].

Table 1. Environment Canada AWS Stations, April-September 2005

Station	Latitude (°N)	Longitude (°W)	Elevation (m)	Frequency
Chesterfield Inlet	63.35	90.73	9.8	Daily
Clyde River	70.48	68.52	26.5	Daily
Coral Harbor	64.19	83.36	62.2	Hourly and daily
Cape Dorset	64.23	76.53	48.2	Daily
Cape Hooper	68.47	66.82	390.1	Hourly
Dewar Lakes	68.65	71.17	526.7	Hourly
Gjoa Haven	68.64	95.85	46.9	Daily
Hall Beach	68.78	81.24	9.1	Hourly and daily
Iqaluit	63.75	68.55	33.5	Hourly and daily
Kugaaruk	68.54	89.80	15.5	Daily
Nanisivik	72.98	84.62	641.9	Daily
Pangnirtung	66.15	65.71	24.1	Daily
Pond Inlet	72.69	77.97	61.6	Daily
Qikiqtarjuaq	67.55	64.03	5.5	Daily
Repulse Bay	66.52	86.22	22.9	Daily
Resolute	74.72	94.98	30.0	Hourly and daily
Taloyoak	69.55	93.58	27.4	Daily

3. Results

3.1. Assessing the Control Run

3.1.1. Temperature

[24] It is first necessary to assess the quality of the WRF Control Run. As mentioned above, summer temperature is the primary control of glacier mass balance in our study region, so we first assess the quality of the model in terms of temperature. Table 1 shows the station names, locations, elevation, and frequency of record available at each site. Figure 1b shows the inner domain and the AWS station locations. There are six available hourly AWS records of temperature in our 10 km resolution domain during April-September 2005. The other 11 stations record daily average temperature.

[25] All WRF temperatures reported below were corrected with a lapse rate of 6 K/km [*Lucas-Picher et al*., 2012] to match the closest WRF grid elevation to the elevation of the AWS to which it is being compared. Figure 2 shows the time series of observed and modeled minimum, maximum, and average 2 m temperatures at the six stations with hourly records. The only inland station available and one of the most poorly simulated locations by the model is Dewar Lakes. Despite a very high and significant correlation between the station and modeled temperature, the WRF Control Run at Dewar Lakes tends to over exaggerate the diurnal temperature cycle. Other stations show more faithful representations of temperatures. Table 2 shows the correlation coefficients, *r*, between 2 m temperature of the WRF Control

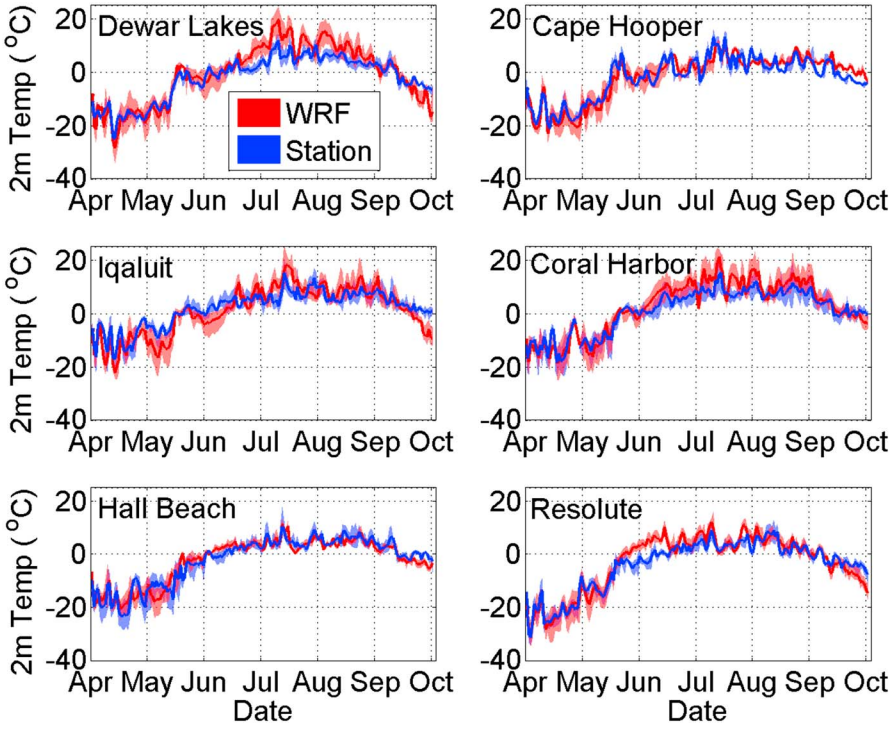

Figure 2. 2 m station (blue) and WRF Control Run (red) mean temperatures (bold lines) and maximum and minimum daily ranges (shaded blue and red). Dewar Lakes, the only inland station on Baffin Island, shows the poorest simulation by WRF.

Table 2. Correlation Coefficient, r, Between WRF Control Run 2 m Temperature and Station Temperature With and Without the Seasonal Cycle Removed

Station	Frequency of Record	Correlation Coefficient, r	Correlation Coefficient, r, After Removing Seasonal Cycle
Chesterfield Inlet	Daily	0.96	0.68
Clyde River	Daily	0.93	0.60
Coral Harbor	Hourly	0.94	0.69
Coral Harbor	Daily	0.96	0.67
Cape Dorset	Daily	0.93	0.59
Cape Hooper	Hourly	0.90	0.42
Cape Hooper	Daily	0.93	0.63
Dewar Lakes	Hourly	0.92	0.51
Dewar Lakes	Daily	0.95	0.64
Gjoa Haven	Daily	0.95	0.61
Hall Beach	Hourly	0.93	0.52
Hall Beach	Daily	0.94	0.43
Iqaluit	Hourly	0.87	0.52
Iqaluit	Daily	0.90	0.53
Kugaaruk	Daily	0.95	0.56
Nanisivik	Daily	0.94	0.40
Pangnirtung	Daily	0.94	0.59
Pond Inlet	Daily	0.95	0.41
Qikiqtarjuaq	Daily	0.93	0.56
Repulse Bay	Daily	0.97	0.66
Resolute	Hourly	0.93	0.57
Resolute	Daily	0.95	0.65
Taloyoak	Daily	0.97	0.61

To compute r, hourly data are sampled every 6 h to match the 6-hourly WRF output. Stations that report hourly also report daily averages, so for these locations, r is calculated for both. All correlations are highly significant, with p values of <0.01 (Student's t-test).

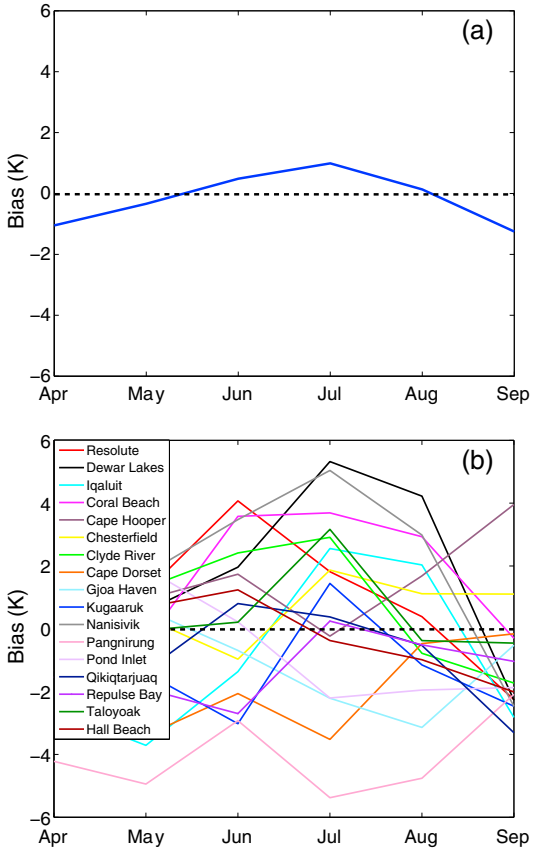

Figure 3. (a) Average monthly bias of WRF Control Run (WRF Control − Station) at all available station locations in the inner domain. (b) Monthly temperature difference between control run and observations for the 17 available station locations. When station curves are above the dotted line, WRF overpredicts the temperature on average for that month at that station.

run and the station records. All correlations presented in Table 2 are statistically significant, with p values of <0.01 (Student's t-test). Some stations have records of both hourly and daily average temperatures, so both are reported in this table. The correlation improves slightly for daily averaged temperature records. Table 2 also shows the correlation coefficient, r, after the seasonal cycle is removed. For the daily average data, this is a measure of how well the model captures the synoptic systems, and for the hourly data, it measures both the ability to model the diurnal cycle and the synoptic systems. The values are all statistically significant, and range between 0.40 and 0.69, suggesting WRF captures both diurnal and synoptic variations with fair accuracy.

[26] We define the temperature bias as the difference between the WRF and the station data temperatures (WRF − Station). The mean monthly WRF Control Run bias at each of the 17 available stations is shown in Figure 3a. The temperature bias of the Control Run, averaged over time and stations, is −0.3 K, consistent with the overall cold bias seen in results from *Wilson et al.* [2011], the cause of which is yet to be determined but is likely due to the land surface model. However, on average WRF tends to overestimate summertime temperatures and underestimate spring and fall season temperatures (Figure 3a). The WRF Control Run produces a strong summertime warm bias at 11 of the 17 locations (Figure 3b). Eight of these 11 stations show the highest overestimate to be in July. The largest bias is at Dewar Lakes with an average July temperature bias of over +5 K.

3.1.2. Clouds

[27] Statistically significant correlations with station temperatures (Table 2) suggest that WRF does a reasonable job of reproducing the daily average temperature (r values >0.90) and the timing of the diurnal cycle (r values between 0.40 and 0.69). However, the model tends to highly exaggerate the diurnal cycle and overestimate summertime average temperatures while underestimating the shoulder season average temperatures. Both of these phenomena were also observed by *Wilson et al.* [2011], who ran the Polar WRF at 60 km resolution for January to December of 2007 over the Arctic System Reanalysis domain. In their follow-up study, *Wilson et al.* [2012] suggested that the diurnal cycle issue was a result of a reduced cloud fraction produced by WRF as compared to satellite observations. This is further supported by excessive incoming shortwave (SW) radiation and low longwave (LW) radiation in the model, both a byproduct of a lack of cloud cover.

[28] To assess if we have the same cloud issue in our simulations, we calculated monthly average cloud fraction for the inner WRF domain, using the polar-adjusted algorithm recommended by *Fogt and Bromwich* [2008], and compared to MODIS Aqua observations (Figure 4a). The difference between WRF and MODIS clouds (Figure 4b) shows that WRF consistently underestimates cloud fraction throughout the 6 month period. Unfortunately, in our case, there are no radiation measurements available at the surface

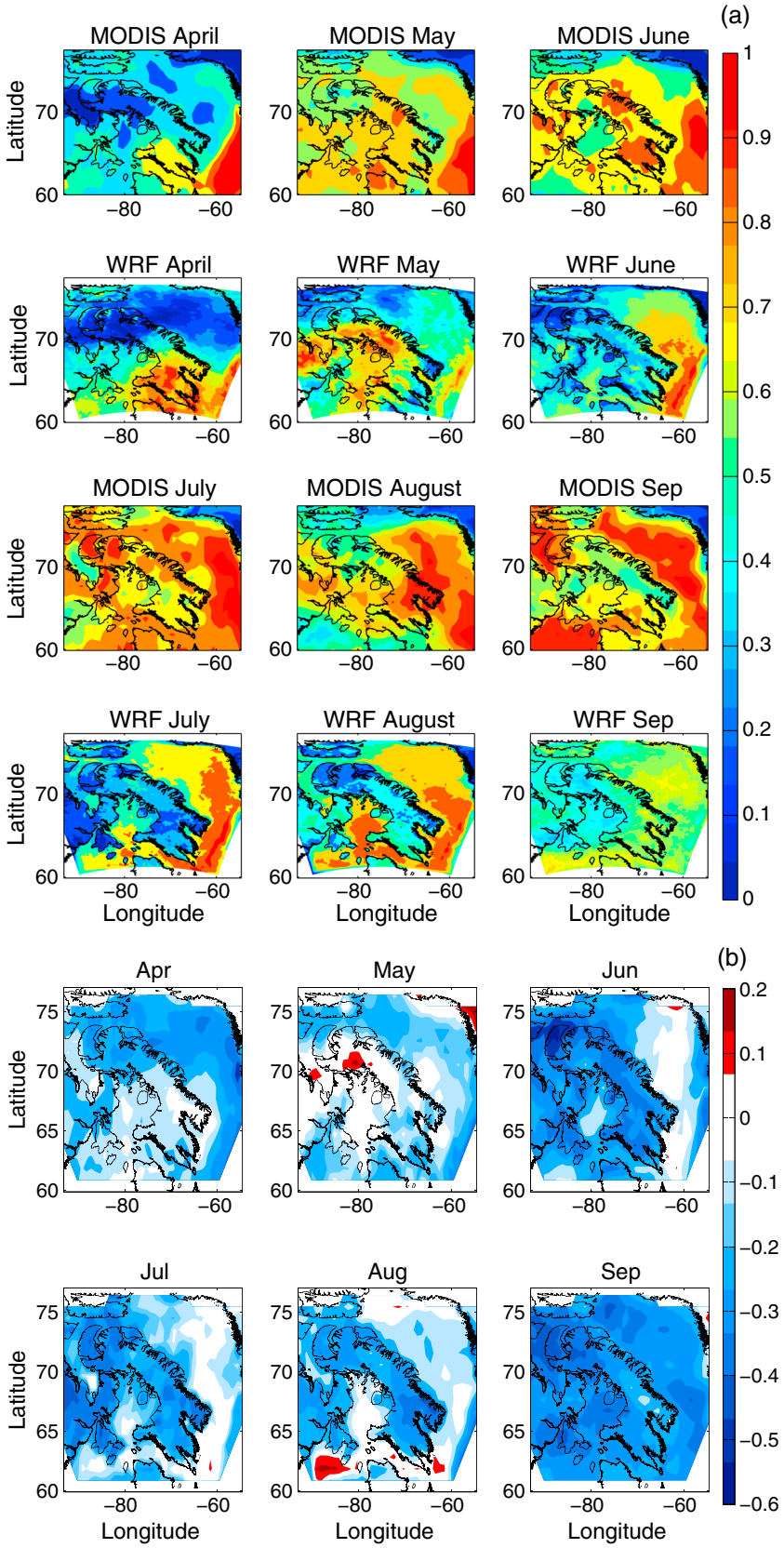

Figure 4. (a) Monthly average cloud fraction from MODIS Aqua observations and WRF Control Run output for 2005, and (b) monthly average cloud fraction difference between WRF and MODIS.

within our domain and time period so we cannot further diagnose the WRF with surface observations. We speculate that the lack of cloud cover would cause an excess in SW radiation, particularly in the summer months when the high latitudes receive many sunlight hours. This effect superimposed on a generally cold biased model [*Wilson et al.*, 2011] produces a warm bias in summer months and cold bias in spring and fall months (Figure 3a). Subsequently, an exaggeration of peak daytime temperatures would likely cause snow to melt too fast in the model. A lack of clouds in the model would also remove any LW warming effect from cloud presence overnight, and thus, minimum daily temperatures are also exaggerated in WRF. This deficiency in WRF is an unfortunate limitation for its use in the Arctic.

[29] To see if cloud simulations could be improved, we conducted several 1 month sensitivity tests. *Wilson et al.* [2012] suggested potential influential factors on cloud fraction amounts, so we independently varied the microphysics scheme (double moment instead of single moment), longwave and shortwave radiation schemes (RRTMG instead of RRTM), and cloud fraction calculation coefficients (standard instead of polar-adjusted). None of these changes significantly increased cloud cover fraction.

3.1.3. Sea Ice and Snow Cover

[30] The time series for sea ice coverage in the inner domain is shown in Figure 5. Sea ice extent is the same across WRF experiments (except for the FixedSI cases where it is held constant) since it is prescribed at each input time by the GFS input. However, there is still a difference between the WRF (GFS) sea ice evolution and the IMS observations, although not as large as that for the snow cover. The GFS input for ice observations shows consistently less sea ice coverage than the IMS observations. This could play a part in the warmer temperatures in the WRF Control run, as less ice would cause warmer temperatures to be advected inland.

[31] Figure 6a shows time series of percent of the inner domain covered in snow for the WRF Control Run, and the two observational datasets, IMS and MODIS CGF. The maximum value of 40% represents full snow cover on land,

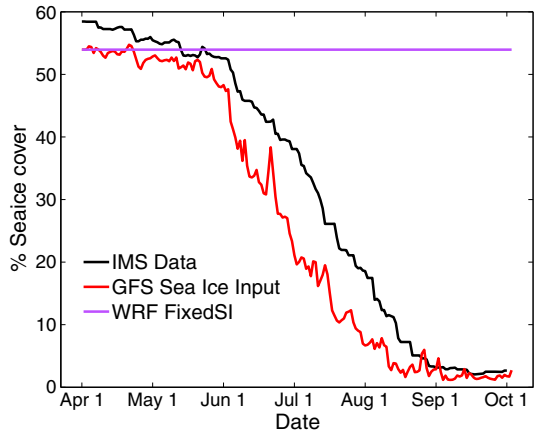

Figure 5. Percent of sea ice cover of the inner domain with time for IMS observations, GFS input to WRF, and the Fixed SI WRF experiment. GFS prescribes WRF's boundary conditions, including that of sea ice distribution, and they are updated every 6 h of model time.

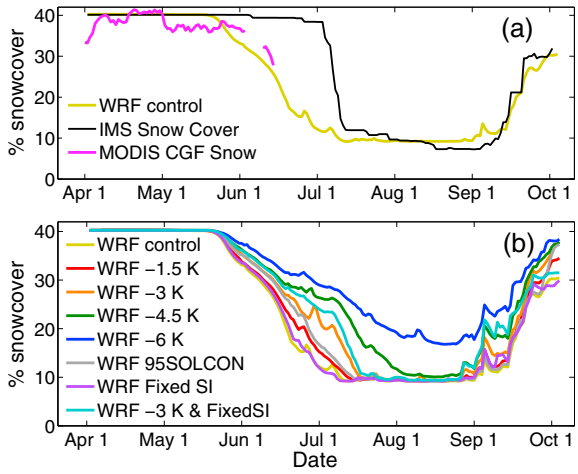

Figure 6. (a) Six month time series of IMS, MODIS CGF, and WRF-modeled snow cover extent expressed as a % of inner domain area. (b) Time series of snow cover % of the inner domain for WRF control run and WRF sensitivity tests.

as there is also ocean (and sea ice) in the domain. The nonzero minimum snow cover extent represents permanent snow and ice fields in the domain. WRF snow cover begins to melt almost a month prior to the IMS observations, but coincides better with the MODIS CGF snow cover time series.

[32] The Noah LSM handles snow evolution in the WRF model. *Hall et al.* [2010] showed that Noah LSM underestimates the snow water equivalent and snowpack depth, which could cause the date of bare ground exposure to be too early in the WRF model output. We checked the WRF snow depths upon model initialization (1 April 2005) and compared to all available snow depth records and found that initial snow cover was accurately represented at initial conditions; however, this does not rule out the notion that as the model progressed, it did not handle the snowpack depth properly. The Noah LSM, in general, has been known to melt the spring snowpack too fast as a result of excessive sublimation and early melt start dates [*Barlage et al.*, 2010]. Given WRF's overestimate of daytime high temperatures, it is likely that in addition to the model's tendency to remove snow too fast, the excess temperatures provide even more residual energy toward snow melt.

[33] In addition to problems with the modeled snow cover, IMS observations are well known for keeping snow on the ground too long. According to *Brown et al.* [2007], IMS and its coarser ancestor, the National Oceanic and Atmospheric Administration (NOAA) snow product, exhibited delays in melt of 22–26 days, and attribute them to elevation effects and frequent cloud cover. *Wang et al.* [2005b] discussed the older NOAA snow product and found that it reported snow cover for up to 4 weeks too long in this region. Cloud cover increased dramatically from May-August (Figure 4), indicating the strong potential for error in the IMS observations and dampened diurnal temperature cycle in the station records. Despite the poor corroboration of the WRF's snow melt timing by the IMS product, the MODIS CGF result is more encouraging. The timing of melt for the MODIS CGF is much more in line with WRF's.

[34] To see if 2005 was an anomaly in the IMS snow observation record, we also looked at 2004 and 2006 IMS data. These years show similar melt onset timing (not shown here) and rate of disappearance for 2004 and 2006, suggesting that 2005 was not an unusually late and sudden snow melt in the IMS records. However, a consistent late-melt bias in the IMS observations cannot be discounted.

[35] We also investigated whether the difference in grid resolution between the IMS observations and WRF grid, and the subsequent snow cover threshold (>50% grid cover = total snow cover) would affect the snow cover results. We tried varying the WRF threshold for snow cover to 20%, 30%, 40%, and 50%, but this produced only minor differences (not shown). Thus, we retained the canonical 50% threshold and concluded that this was likely only a minor factor in the difference between WRF and IMS snow melt timing.

[36] In more than one instance, WRF cannot resolve very narrow and steep fjords, particularly on the east coast of the island, where some stations lay. The discrepancy between modeled and station elevation likely plays another role in explaining discrepancies between observed and modeled temperature and snow cover.

[37] WRF is a state-of-the-art regional climate model, but its issues with clouds, 2 m temperature, and snow are an ongoing area of research [*Hines and Bromwich*, 2008; *Hines et al*., 2011; *Wilson et al*., 2011, 2012]. Despite the inherent problems with the WRF Control Run, we proceed to assess our snow sensitivity experiments by considering relative changes to the Control Run.

3.2. WRF Experiments

3.2.1. Radiation Versus Advection

[38] Since we are seeking to evaluate the snow sensitivity in the model, the WRF experiments are evaluated below, predominantly in terms of how effective they are at retaining snow on the ground during the 6 month simulation. First, though, we look at how the model performance (Bias and Root Mean Square Error (RMSE)) is affected by the WRF experiments by comparing station temperature records to each WRF temperature simulation at that location. 6-hourly temperature bias is strongly a function of model run (which is to be expected with the given experiments), while RMSE is affected more by station location (Figure 7a). Using average daily temperatures instead of 6-hourly records (Figure 7b), the bias is unchanged, but the RMSE is systematically reduced. Thus, the model does a better job at computing daily average temperature as compared to the diurnal cycle, which tends to exhibit over-exaggerated variability. Figure 7c shows the same as Figure 7b, but with additional stations that only record daily average temperature. The larger the experimental temperature perturbation, the higher the RMSE becomes. The bias values here are not just a result of the experimental temperature perturbation, but would also include effects from the difference between the closest WRF grid elevation and the actual station elevation. Next, we examine the *effective* temperature change inland as a result of the perturbation experiments. Since the temperature changes in the temperature perturbation cases are only applied to the lateral boundaries of the parent domain every 6 h of model time, the temperature is not expected to propagate in full magnitude toward the center of the inner domain. We examined the effective monthly average temperature change at all grid cells of the inner domain as a result of each experiment for two elevation categories, 0–0.5 m (ocean grid cells predominantly) and 0.5–2900 m (land). The WRF −1.5 K, −3 K, −4.5 K, and −6 K temperature experiments are not realized in full magnitude at the beginning of the runs, particularly at sea level, as seen in Figures 8a and 8b. This is important to keep in mind throughout the rest of sections 3 and 4, as the effective temperature change is less than that imposed on the boundaries, so snow extent may not be as affected as one would expect from a full 1.5 K, 3 K, 4.5 K, or 6 K cooling.

[39] In Figures 8a and 8b, all experiments show decay toward zero bias in the effective temperature difference from the Control Run with time, although the runs with fixed sea ice deviate from this trend after July, as we discuss later. Figure 8b (land) shows a less pronounced decay toward zero than Figure 8a (ocean), partly because it is masked by a dip in July for the −4.5 K and −6 K cases, which has to do with the presence of more snow on the ground in these runs and will be explained in more detail later.

[40] In both Figures 8a and 8b, a robust feature of the FixedSI runs stands out, where temperature differences plummet in September. This feature is particularly strong in the sea level panel results (Figure 8a) which makes sense since the sea surface temperatures and sea ice are fixed to 1 April conditions for the whole experiment period, and the surface temperature of sea ice does not have the lower bound that open water has. However, we do see a very strong cooling signal of about 7 K in September at elevations above 0.5 m (Figure 8b) for the FixedSI run, implying a very strong influence of the sea ice presence on inland temperatures. In the Control Run, September has the minimum sea ice distribution, and the sea surface temperatures are otherwise warm compared to colder temperatures on land. Thus, imposing sea ice stunts an otherwise energy-rich ocean from providing warmth inland. Instead, extremely cold temperatures are simulated by the model. The slight warming during July in the FixedSI run in Figure 8b is likely a result of the large overestimates of near-surface temperatures on land by the model. These high temperatures (at Dewar Lakes, the Control Run sometimes reached over 10 K difference between modeled and observed daily highs in July) outcompete the cooling effects of the expanded sea ice. Figure 8b shows a robust cooling in the −6 K case in July. This is likely attributed to the anomalous snow cover (Figure 6b), which would reflect incoming solar radiation and further cool the local atmosphere and dedicate more energy to melting snow instead of warming the atmosphere [*Williams*, 1978b]. To further explore this, we compare the available snow depth observations from in situ stations to snow cover in the WRF −6 K experiment. We find that the station locations that experienced delayed bare ground exposure in the WRF −6 K experiment until at least mid-July (often later) are also the stations that exhibited anomalous cooling by at least 5 K compared to the Control Run. Thus, a feedback is induced where colder temperatures can produce anomalous snow cover, which in turn produce further cooling.

[41] It is of interest to examine whether the sum of the WRF −3 K and FixedSI runs produces the equivalent temperature effect as the run where the two effects are combined simultaneously (WRF −3 K and FixedSI). The insets in

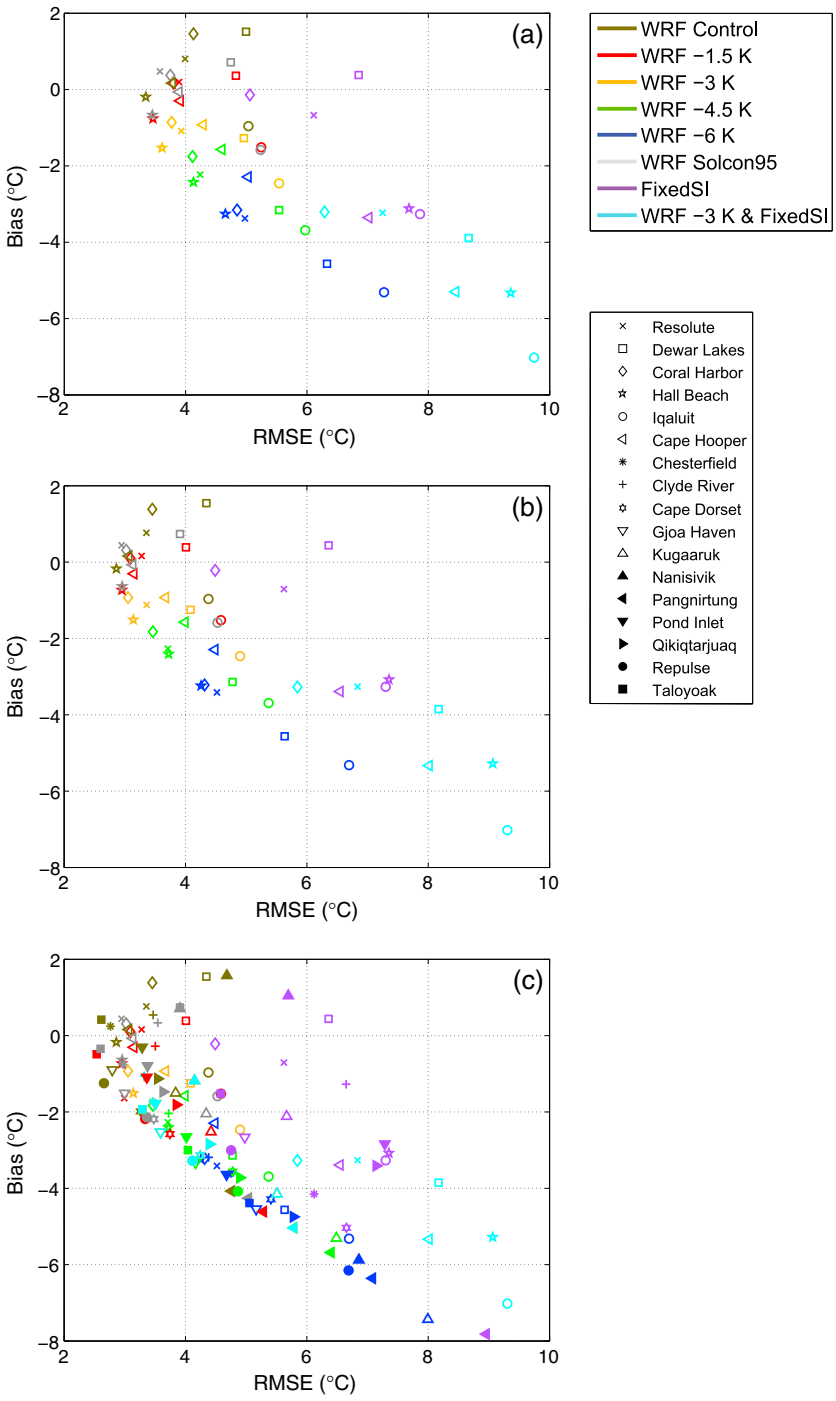

Figure 7. (a) Bias versus RMSE between station and WRF for 2 m temperature (6 hourly) for April-September 2005, (b) daily average temperature for same stations, and (c) additional stations with daily average temperature records.

Figures 8a and 8b show the difference between the sum of the −3 K run and the FixedSI run, and the WRF −3 K and FixedSI run in which both perturbations act in concert. All months in the insets show a positive difference which increases as the simulations progress. This shows that the run which combines the two perturbations at once has a greater cooling effect than the sum of the constituent parts run independently and that this effect increases over time. The advection of the perturbed temperatures over sea ice keeps the temperatures cooler than if the surface were open ocean. This effect is amplified in the autumn months when open ocean otherwise provides energy to the atmosphere.

[42] Next, we examine how snow extent is affected by the WRF experiments. It is clear from Figure 6b that the experiments affect the rate of melt much more than the date of melt onset. The snow accumulation in the fall season shows that WRF captures the synoptic systems that cause precipitation and that the experiments cause more precipitation in the

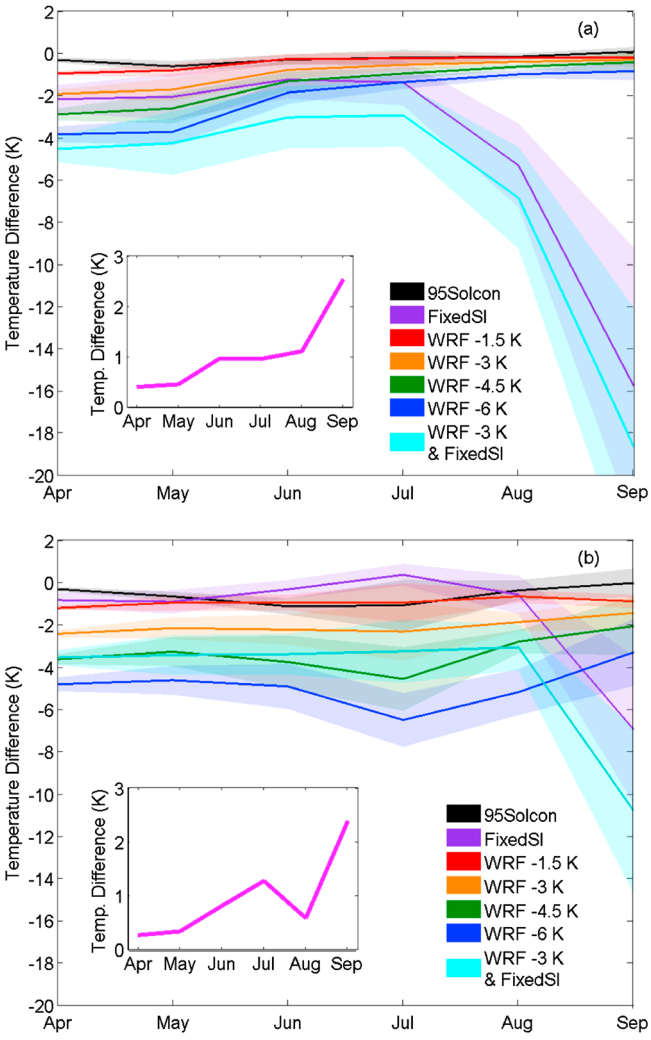

Figure 8. Monthly average temperature difference between WRF Control Run and sensitivity experiments for grid cells at elevations between (a) 0 and 0.5 m (predominantly ocean grid points) and (b) 0.5 m and 2900 m (land only grid points). Insets have same axes as main plots, and show the difference between the sum of the WRF 3K run and FixedSI run ([WRF −3 K] + [FixedSI]), and the WRF 3K and FixedSI run ([WRF −3 K and FixedSI]). Positive values indicate that the [WRF −3K and FixedSI] run has a greater cooling effect than the sum of the constituent parts run independently.

form of snow than the Control Run. The 95SOLCON case begins to melt very similarly to the −3 K case, but deviates mid-melt season, arriving at a total bare ground situation before the −3 K case. The combined −3 K and FixedSI run is more effective at keeping snow cover on the ground longer during the spring thaw compared to the regular −3 K case; however, by mid-July, it reaches the same minimum level snow cover. The effects of the 95% solar constant on surface radiation are not as strong in the polar regions as at the equator. At summer solstice, for example, such a reduction of the solar constant at the equator would result in a daily average change in insolation of −23.8 W/m^2, whereas at 67°N, the change would only be −18.9 W/m^2. This equates to about a 20% difference between the average daily insolation on June 21 at the equator and at 67°N. Thus, the effect of changing the solar constant is not realized as strongly at high latitudes. Perhaps more importantly though, as was mentioned in section 1, the boundary conditions feeding WRF are not subjected to a reduction in solar radiation, so the response of the climate is limited. As a result, advection dominates and radiation has very little impact. It is then not surprising that the 95SOLCON experiment does not produce more severe changes, despite the rather severe drop in radiation. Table 3 gives the minimum snow cover of the inner domain for each run. The −3 K, −4.5 K, −6 K, and −3 K and FixedSI runs are the cases where the snow does not melt to the same as the Control Run. The −6 K run is the only run that substantially increases (almost 50% increase in area snow coverage compared to the Control Run) the snow cover extent at summer's end, showing that this advective perturbation is more effective at inducing a snow cover change than the 5% radiation change, at least in our simulations.

3.2.2. WRF Temperature Experiments

[43] Since we are ultimately interested in the sensitivity of snow extent to temperature perturbations, particularly when the minimum snow cover is reached in each run, we examine the relative changes of snow cover extent as a function of WRF temperature experiments (WRF −1.5 K, −3 K, −4.5 K, and −6 K). Figure 9 illustrates that on the minimum snow extent day, the WRF −6 K case keeps snow cover north of 66°N, west from the north central Baffin Island plateau region, and into the Northwest peninsula of the island. Melville Peninsula, to the west of Baffin Island, also retains a good amount of snow cover. This agrees quite well with the LIA snow line regions demarked by *Williams* [1978a] from sparse lichen-covered areas, who noted that the LIA snow extended more in the North than the South, and from the north central plateaus, there was a distinct lowering to the west. Thus, despite problems with the 2 m temperature and the Noah LSM, WRF can realistically simulate where snow cover is most likely to expand, in effect characterizing the regional snow sensitivity.

[44] Figure 10 shows snow cover percent as a function of 50 m elevation bands for each cooling experiment and the Control Run on the minimum snow extent day, excluding Greenland and all latitudes below 66°N. There is almost no change between the Control Run and the −1.5 K and −3 K minimum snow extent for any elevation range. The −4.5 K and −6 K cases, however, show different departures from the Control, –1.5 K and −3 K runs. The Control Run shows that full snow coverage exists above about 1200 m elevation, agreeing with current field estimates, but that patchy snow exists below that. Defining the equilibrium line altitude from

Table 3. Minimum Snow Cover Percent of Inner Domain for Each WRF Run

WRF Run	Minimum Snow Cover (%)
−6 K	17.0
−4.5 K	10.1
−3 K	9.4
−1.5 K	9.2
Control	9.2
95SOLCON	9.2
FixedSI	9.2
−3 K and FixedSI	9.4

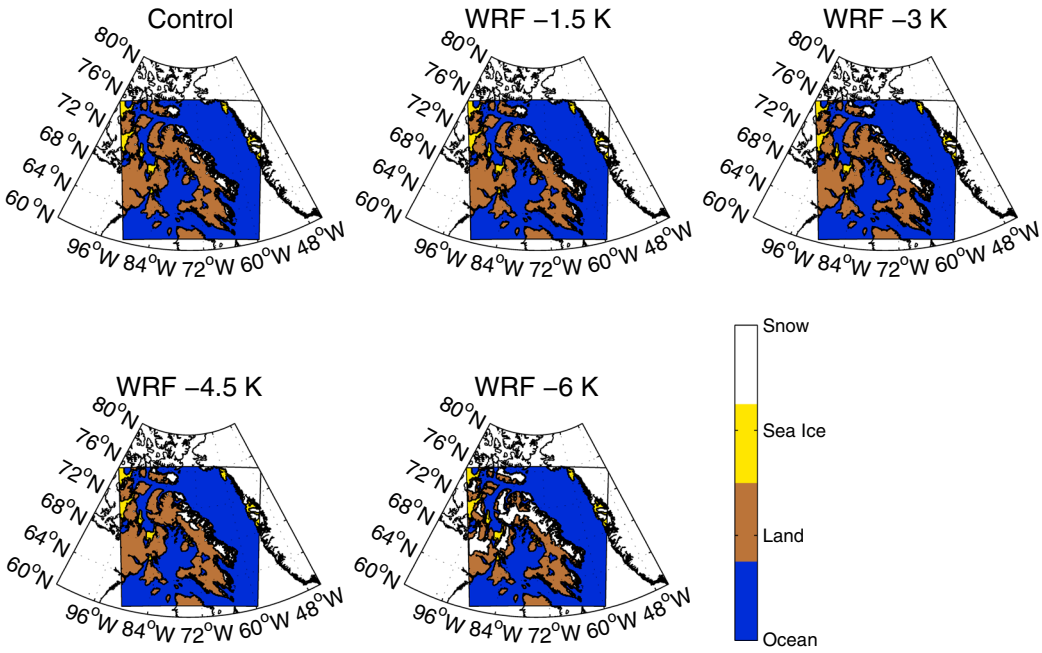

Figure 9. Minimum snow extent reached for each cooling experiment.

this plot becomes problematic, since there is not a clear step change from no snow to full snow cover, but rather a gentler transition from bare ground to full snow cover. Indeed, the slope is steeper for the Control, –1.5 K and –3 K runs, than the colder runs, suggesting that the snow cover is not just a function of elevation but of other considerations such as terrain aspect and local temperature.

[45] For a given snow cover percent threshold, it is possible to extract snow line elevation and determine its sensitivity to temperature. We show the minimum snow line elevation is shown as a function of the average 6 month temperature difference between the Control Run and the given cooling experiment (Figure 11). There are no changes between the Control Run, –1.5 K run and the –3 K run, for reasons outlined in sections 3.1.1 and 3.1.3, so if we take the slope of the coldest three points, we find the sensitivity of the snow line for the given threshold. The corresponding sensitivities are listed beside the curves in Figure 11. The choice of threshold affects the sensitivity result, and the elevation range of interest. The 50% cover threshold shows the largest change between WRF runs in snow cover. On average, it produces a sensitivity of about 7 K/km, and is relevant to elevations in the range of 300–700 m elevation, coinciding with the elevation range of Baffin Island's north central plateau. This value is also the upper end of the free-air moist adiabatic lapse rate, the value often used to extrapolate from station temperatures in this region [*Gardner et al.*, 2009].

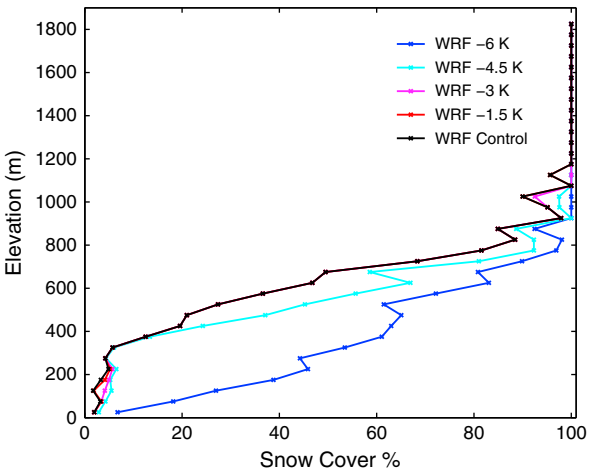

Figure 10. Fraction of snow-covered area (based on ≥50% threshold for each grid cell snow cover) for elevation bands, in 50 m elevation intervals, on the minimum snow extent day, and excluding Greenland and latitudes south of 66°N.

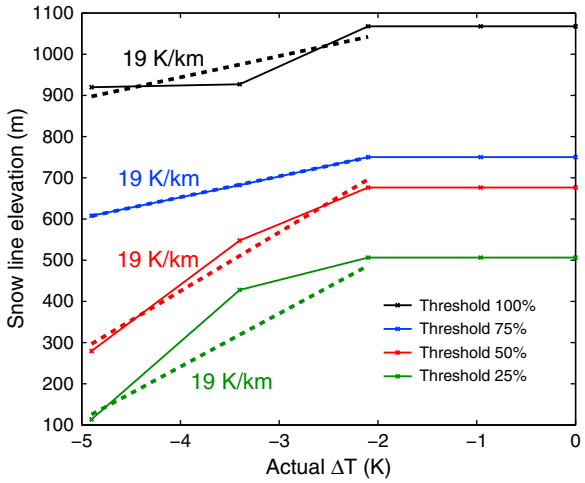

Figure 11. Minimum snow line elevation, as defined by the threshold of how much of each elevation band is covered in snow, as a function of average 6 month temperature difference between the Control Run and the given cooling experiment. The associated lapse rates found from the slope of the best fit line to the coldest three points are shown for each curve.

The minimum snow line elevation change between the Control Run and the −6 K run given the 50% snow cover threshold is 350 m, the upper end of what was observed by *Miller et al*. [2012].

[46] Even though an average temperature decrease of roughly 2K did not impact the snow cover, it is not clear how much of this cooling was necessary to produce the observed snow changes. We can only conclude, then, that the magnitude of average temperature change that caused the modeled snow cover change in the WRF −6 K case is as much as −4.9 K or as little as −2.8 K, or otherwise -3.9 ± 1.1 K. Thus, given the 50% snow cover threshold, with an average temperature decrease of -3.9 ± 1.1 K, WRF is capable of producing an abrupt snow line elevation change within only one summer season which is comparable in magnitude to that observed during the LIA.

4. Discussion

[47] Our major findings can be summarized as follows. The WRF Control Run shows significant correlations with observed temperature records at all stations. Part of this strong agreement is related to the forcing of WRF with a global model that assimilates observations and to the spectral nudging of the *u* and *v* wind fields above the boundary layer (section 2.1). The diurnal cycle is often highly exaggerated, with differences in peak daily temperatures up to 10 K, but daily average temperatures are better predicted than the diurnal temperature cycle. The lack of cloud cover predicted by the model is a likely reason for these problems, an issue that has been observed in other WRF studies in the Arctic [*Wilson et al*., 2012]. At more than half of the stations, the WRF Control Run tends to overestimate summer temperatures and underestimate spring and fall temperatures. The WRF Control Run begins to lose snow cover about a month earlier than the IMS data suggest, but matches very well with the timing of MODIS CGF snow cover product. This discrepancy with IMS could be a result of errors in observations (e.g., cloud cover obstruction during IMS data collection) or a tendency for the Noah LSM to sublimate or melt snow more readily than in the real world [*Wang et al*., 2005a; *Brown et al*., 2007; *Barlage et al*., 2010].

[48] Despite issues with the WRF Control Run, relative changes between the Control Run and the experiments provide insights into the sensitivity of this particular environment to sudden changes in temperature, sea ice expansion, and solar radiation. The 95SOLCON, FixedSI, and −3 K and FixedSI runs were unable to cool the domain enough to retain more snow than the Control Run. However, the FixedSI run did exhibit a robust average near-surface cooling of about 7 K over land in September, suggesting that a sudden expansion of sea ice has quite significant effects inland in seasons when the ocean is otherwise heating the atmosphere. This hints at the strong potential for expanded sea ice to affect inland temperature and snow cover beyond the model's end date of 30 September. The run which applied the −3 K and FixedSI perturbations simultaneously (−3 K and FixedSI) showed a greater cooling effect on inland temperatures than the addition of the two independent constituent runs (WRF −3 K) + (FixedSI), and this effect was amplified over the course of the 6 month simulation. Greater sea ice coverage would be expected in colder years so one would expect them to interact, which, as this experiment suggests, would lead to cooling greater than the sum of the parts. The temperature sensitivity experiments (WRF −1.5 K, –3 K, –4.5 K, and –6 K), applied at the boundaries of the outer domain, did not propagate to the inner domain in their full magnitude, and this effect became more evident in the later months of the runs. The WRF experiments influenced the rate of melt, but the date of melt onset was relatively unchanged between runs. The only runs successful in substantially suppressing the snow line were WRF −4.5 K and WRF −6 K. The WRF −6 K run showed increased snow cover north of 66°N, moving west into the north central plateau and NW peninsulas of Baffin Island, and into Melville Peninsula in Nunavut. These regions coincide with the LIA snow line outlined by *Williams* [1978a], suggesting that the WRF does a realistic job of highlighting regional sensitivity to snow line change. The amount of actual cooling necessary to expand the area of snow cover by 50% from the Control Run to the −6 K run is -3.9 ± 1.1 K.

[49] Using 50 m elevation bands, snow cover varies continuously from bare ground to full snow cover. Thus, there is not one obvious choice which defines the snow line, and the snow line's sensitivity to temperature change depends on this choice. We find that the sensitivity of snow line to temperature is greatest, 7 K/km, when the snow line is defined as 50% snow cover. Given this definition, the minimum snow line elevation difference between the Control Run and the −6 K run is 350 m. Such a change in elevation is on the upper end of what was observed by *Miller et al*. [2012]. Thus, the WRF model can lower the snowline by comparable elevation changes seen during the descent into the LIA, in only one season, with an average temperature decrease from current temperatures by -3.9 ± 1.1 K. Given the WRF's sensitivity of 7 K/km, and *Miller et al*.'s [2012] data which show two events where the snow line elevation changed by 240 m and 340 m, a temperature decrease of 1.7 and 2.4 K would be necessary to cause such a change.

5. Conclusions

[50] In the scenario suggested by *Miller et al*. [2012], successive volcanic eruptions suppressed summer temperatures enough to cause expanded snow cover and sea ice. In our high-resolution WRF simulations, we examined the effect that a sudden suppression of temperatures, reduction of incoming solar radiation, and expansion of sea ice might have on snow cover after only one summer season on Baffin Island. Despite WRF's inherent issues with cloud cover, diurnal temperature variations, and snow cover, the simulations still produced reasonable estimates of snow line sensitivity. In particular, the WRF model showed excellent correspondence between where snow expansion was observed in the −6 K case, and where *Williams* [1978a] demarked the LIA snow line. We found that the region responding with most sensitivity to a summer temperature reduction of -3.9 ± 1.1 K from the Control Run was the northern Baffin Island plateau between 400 and 700 m elevation, where snowline lowered by 350 m, similar to the reconstructed snowline of Williams [1978a].

[51] Applying the maximum snow line sensitivity we observed in the WRF model (7 K/km) to the *Miller et al*. [2012] data, which show snow line lowering by 240–340 m,

we find that a temperature decrease from current conditions of 1.7–2.4 K would be necessary to reproduce what they observed. By comparison, applying the mean ablation season lapse rate of 4.9 K/km derived from ice sheets in the Canadian Arctic [*Gardner et al*., 2009] suggests that even less of a temperature decrease, 1.2–1.7 K, could be necessary to produce the observed snow line descent. Our WRF results also showed that expanded sea ice has the strong potential to reduce inland temperatures.

[52] Proxy records from Devon and Agassiz Ice Caps near Baffin Island show summer temperature anomalies from 1400 to 1700 CE that were about 6 K cooler than the 1860–1959 mean [*Bradley and Jones*, 1993]. Arctic-averaged decadal summer temperature anomaly estimates based on a composite of proxy records shows about 1.5 K difference between the LIA and current values [*Kaufman et al*., 2009]. Thus, if Baffin regional temperatures during the LIA were roughly 2 K lower than present (which is reasonable, given the proxy records), and there was a more extensive sea ice cover; this together would have been enough to perpetuate an ice sheet on Baffin Island throughout the LIA.

[53] It is important and useful to highlight the gaps in performance in the high-resolution modeling and observations in high latitude applications, particularly for those interested in evaluating snow cover. The WRF's poor simulations of diurnal temperatures, particularly at the inland sites, the lack of cloud cover produced in an otherwise overcast region, and the land surface model's tendency to melt snow too fast leave the model results wanting. On the other hand, satellite observations of snow cover in the high latitudes are flawed as well, given the high frequency of cloud cover in the summer season. The combination of error-prone observations and model output tend to bring one to an enigmatic crossroad. However, in an application such as this, we have shown that looking at relative changes can yield valuable information about how the model works, and what that might mean in the real world.

[54] **Acknowledgments.** High-performance computing support was provided by NCAR's Computational and Information Systems Laboratory, sponsored by the National Science Foundation. We thank Gifford Miller, David Robinson, and Michael Barlage for valuable discussions, and Aaron Wilson for his input on cloud fraction calculations. We also thank three reviewers for their thoughtful comments and suggestions which led to a stronger manuscript. This work was supported by NSF grants ARC-0908834 and AGS-1157525.

References

Anderson, R., G. Miller, J. Briner, N. Lifton, and S. DeVogel (2008), A millennial perspective on arctic warming from 14C in quartz and plants emerging from beneath ice caps, *Geophys. Res. Lett.*, *35*(1), L01502, doi:10.1029/2007GL032057.

Andrews, J. T., R. G. Barry, R. S. Bradley, G. H. Miller, L. D. Williams (1972), Past and present glaciological responses to climate in eastern Baffin Island, *Quaternary Res.*, *2*(3), 303–314.

Barlage, M., F. Chen, M. Tewari, K. Ikeda, D. Gochis, J. Dudhia, R. Rasmussen, B. Livneh, M. Ek, and K. Mitchell (2010), Noah land surface model modifications to improve snowpack prediction in the Colorado Rocky Mountains, *J. Geophys. Res.*, *115*, D22101, doi:10.1029/2009JD013470.

Bradley, B.S., and P.D. Jones (1993), 'Little Ice Age' summer temperature variations: Their nature and relevance to recent global warming trends, *Holocene*, *3*(4), 367–376.

Brown, R., C. Derksen, and L. Wang (2007), Assessment of spring snow cover duration variability over northern Canada from satellite datasets, *Remote Sens. Environ.*, *111*(2–3), 367–381.

Brown, R., C. Derksen, and L. Wang (2010), A multi-data set analysis of variability and change in Arctic spring snow cover extent, 1967–2008, *J. Geophys. Res.*, *115*(D16), D16111, doi:10.1029/2010JD013975.

Cassano, J. J., M. E. Higgins, and M. W. Seefeldt (2011), Performance of the Weather Research and Forecasting (WRF) model for month-long pan-Arctic simulations, *Mon. Wea. Rev.*, *139*, 3469–3488, doi:10.1175/MWR-D-10-05065.1.

Catchpole, A.J.W., and I. Hanuta (1989), Severe summer ice in Hudson Strait and Hudson Bay following major volcanic eruptions, 1751 to 1889 A.D., *Climatic change*, *14*, 61–79.

Chen, F., and J. Dudhia (2001), Coupling an advanced land surface-hydrology model with the Penn State-NCAR MM5 modeling system. Part I: Model implementation and sensitivity, *Mon. Wea. Rev.*, *129*(4), 569–585.

Chou, M.-D., and M. Suarez (1994), An efficient thermal infrared radiation parameterization for use in general circulation models, NASA Tech. Memo., 104606, 85 pp.

Fogt, R. L., and D. H. Bromwich (2008), Atmospheric moisture and cloud cover characteristics forecast by AMPS, *Weather Forecast.*, *23*, 914–930, doi:10.1175/2008WAF2006100.1.

Gardner, A. S., M. J. Sharp, R. M. Koerner, C. Labine, S. Boon, S. J. Marshall, D. O. Burgess, D. Lewis (2009), Near-surface temperature lapse rates over Arctic glaciers and their implications for temperature downscaling, *J. Clim.*, *22*, 4281–4298, doi:10.1175/2009JCLI2845.1

Geirsdóttir, Á., G. H. Miller, T. Thordarson, and K. Ólafsdóttir (2009), A 2000 year record of climate variations reconstructed from Haukadalsvatn, west Iceland, *J. Paleolimnol.*, *41*(1), 95–115, doi:10.1007/s10933-008-9253-z

Greuell, W., and R. Böhm (1998), 2 m temperatures along melting mid-latitude glaciers, and implications for the sensitivity of the mass balance to variations in temperature, *J. Glaciol.*, *44*, 9–20.

Hall, D. K., G. A. Riggs, J. L. Foster and S. V. Kumar (2010), Development and evaluation of cloud-gap-filled MODIS daily snow-cover product, *Remote Sens. Environ.*, *114*(3), 496–503, doi:10.1016/j.rse.2009.10.007.

Hines, K. M., D. H. Bromwich, L.-S. Bai, M. Barlage, and A. G. Slater (2011), Development and testing of Polar WRF. Part III. Arctic land. *J. Clim.*, *24*, 26–48, doi:10.1175/2010JCLI3460.1.

Hines, K. M. and D. H. Bromwich, (2008), Development and testing of Polar Weather Research and Forecasting (WRF) model. Part I: Greenland ice sheet meteorology, *Mon. Wea. Rev.*, *136*, 1971–1989, doi:10.1175/2007MWR2112.1.

Hong, S., J. Dudhia, and S. Chen (2004), A revised approach to ice microphysical processes for the bulk parameterization of clouds and precipitation, *Mon. Wea. Rev.*, *132*, 103–120.

Hong, S., Y. Noh, and J. Dudhia (2006), A new vertical diffusion package with an explicit treatment of entrainment processes, *Mon. Wea. Rev.*, *134*(9), 2318–2341, doi:10.1175/MWR3199.1.

Ikeda, K., et al. (2010), Simulation of seasonal snowfall over Colorado, *Atmos. Res.*, *97*(4), 462–477, doi:10.1016/j.atmosres.2010.04.010.

Ives, J. D., (1962), Indications of recent extensive glacierization in north-central Baffin Island, N.W.T., *J. Glaciol.*, *4*, 197–205.

Kain, J. (2010), The Kain-Fritsch convective parameterization: An update, *J. Appl. Meteor.*, *43*(1), 170–181, doi:10.1175/1520-450(2004)043<0170:TKCPAU>2.0.CO;2.

Kaufman, D.S., et al. (2009), Recent warming reverses long-term Arctic cooling, *Science*, *325*, 1236–1239.

Koerner, R. M. (2005), Mass balance of glaciers in the Queen Elizabeth Islands, Nunavut, Canada, *Ann. Glaciol.*, *42*, 417–423.

Lucas-Picher, P., M. Wulff-Nielsen, J. Christensen, G. Aalgeirsdóttir, R. Mottram, and S. Simonsen (2012), Very high resolution regional climate model simulations over Greenland: Identifying added value, *J. Geophys. Res.*, *117*(D2), D02108, doi:10.1029/2011JD016267.

McCormick, M., L. Thomason, and C. Trepte (1995), Atmospheric effects of the Mt. Pinatubo eruption, *Nature*, *373*(6513), 399–404, doi:10.1038/373399a0.

Miguez-Macho, G., G. Stenchikov, and A. Robock (2004), Spectral nudging to eliminate the effects of domain position and geometry in regional climate model simulations, *J. Geophys. Res.*, *109*, D13104, doi:10.1029/2003JD004495.

Miller, G. H. (1973), Late quaternary glacial and climatic history of northern Cumberland Peninsula, Baffin Island, N.W.T., Canada, *Quaternary Res.*, *3*, 561–583.

Miller, G. H., et al. (2010), Temperature and precipitation history of the Arctic, *Quaternary Sci. Rev.*, *29*(15–16), 1679–1715, doi:10.1016/j.quascirev.2010.03.001.

Miller, G. H., et al. (2012), Abrupt onset of the little ice age triggered by volcanism and sustained by sea-ice/ocean feedbacks, *Geophys. Res. Lett.*, *39*(2), L02708, doi:10.1029/2011GL050168.

Mlawer, E., S. Taubman, P. Brown, M. Iacono, and S. Clough (1997), Radiative transfer for inhomogeneous atmospheres: RRTM, a validated correlated-k model for the longwave, *J. Geophys. Res.*, *102*(D14), 16, 663–16, doi:10.1029/97JD00237.

National Ice Center (2008), IMS daily Northern Hemisphere snow and ice analysis at 4 km and 24 km resolution. (National Snow and Ice Data

Center Boulder, CO). Digital media. http://nsidc.org/data/docs/noaa/g02156_ims_snow_ice_analysis

Robock, A. (2000), Volcanic eruptions and climate, *Rev. Geophys.*, *38*, 191–219.

Skamarock, W., et al. (2008) A description of the advanced research WRF version 3, *NCAR Tech*. *Note NCAR/TN-475+ STR*.

Wang, L., M. Sharp, R. Brown, C. Derksen, and B. Rivard (2005a), Evaluation of spring snow covered area depletion in the Canadian arctic from NOAA snow charts, *Remote Sens. Environ.*, *95*(4), 453–463, doi:10.1016/j.rse.2005.01.006.

Wang, L., M. Sharp, B. Rivard, S. J. Marshall, and D. Burgess (2005b), Melt season duration on Canadian Arctic ice caps, 2000–2004, *Geophys. Res. Lett.*, *32*(19), L19502, doi:10.1029/2005GL023962.

Williams, L. D. (1978a), The Little Ice Age glaciation level on Baffin Island, Arctic Canada, *Palaeogeogr. Palaeoclim.*, *25*, 199–207.

Williams, L. D. (1978b), Ice-sheet initiation and climatic influences of expanded snow cover in Arctic Canada, *Quaternary Res.*, *10*(2), 141–149.

Wilson, A., D. Bromwich, and K. Hines (2011), Evaluation of Polar WRF forecasts on the arctic system reanalysis domain: Surface and upper air analysis, *J. Geophys. Res.*, *116*, D11112, doi:10.1029/2010JD015013.

Wilson, A., D. Bromwich, and K. Hines (2012), Evaluation of Polar WRF forecasts on the Arctic System Reanalysis domain: 2. Atmospheric hydrologic cycle, *J. Geophys. Res.*, *117*, D04107, doi:10.1029/2011JD016765.

Zhong, Y., G. H. Miller, B. Otto-Bliesner, M. Holland, D. Bailey, D. Schneider, and A. Geirsdottir (2010), Centennial-scale climate change from decadally-paced explosive volcanism: A coupled sea ice-ocean mechanism, *Clim. Dynam.*, 1–15, doi:10.1007/s00382-010-0967-z.